Analyst

Accepted Manuscript

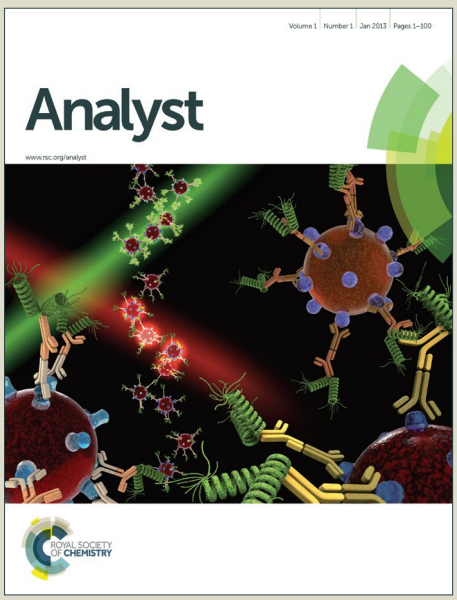

ROYAL SOCIETY OF CHEMISTRY

www.rsc.org/analyst

A uniform measurement expression for cross method comparison of nanoparticle aggregate size distributions.

Agnieszka Dudkiewicz*[1, 2], Stephan Wagner[3], Angela Lehner[4], Qasim Chaudhry[1], Stéphane Pietravalle[1], Karen Tiede[1], Alistair B.A. Boxall[2], Guenter Allmaier[4], Dirk Tiede[5], Ringo Grombe[6] Frank von der Kammer[3], Thilo Hofmann[3] and Kristian Mølhave[7]

[1]The Food and Environment Research Agency, Sand Hutton, York Y041 1LZ, UK.

[2]The University of York, Heslington, York, YO10 5DD, UK.

[3]Department of Environmental Geosciences, University of Vienna, Althanstrasse 14, A-1090 Vienna, AT.

[4]Reasearch group Bio- and Polymer Analysis, Institute of Chemical Technologies and Analytics, Vienna University of Technology, Getreidemarkt 9/164 A-1060 Vienna, AT.

[5]Department of Geoinformatics - Z_GIS, University of Salzburg, Schillerstr. 30, A-5020 Salzburg, AT.

[6]Joint Research Centre, Institute for Reference Materials and Measurements, Retieseweg 111, Geel 2440, BE.

[7]Deptartment of Micro and Nanotechnology, Technical University of Denmark, Lyngby 2800, DTU Bldg 345b, DK.

**Corresponding author, e-mail address: agnieszkaidudkiewicz@gmail.com*

Abstract

Available measurement methods for nanomaterials are based on very different measurement principles and hence produce different values when used on aggregated nanoparticle dispersions. This paper provides a solution for relating measurements of nanomaterials comprised of nanoparticle aggregates determined by different techniques using a uniform expression of a mass equivalent diameter (MED). The obtained solution is used to transform into MED the size distributions of the same sample of synthetic amorphous silica (nanomaterial comprising aggregated nanoparticles) measured by six different techniques: scanning electron microscopy in both high vacuum (SEM) and liquid cell setup (Wet-SEM); gas-phase electrophoretic mobility molecular analyzer (GEMMA); centrifugal liquid sedimentation (CLS); nanoparticle tracking analysis (NTA); and asymmetric flow field flow fractionation with inductively coupled plasma mass spectrometry detection (AF4-ICP-MS). Transformed size distributions are then compared between the methods and conclusions drawn on methods' measurement accuracy, limits of detection and quantification related to the synthetic amorphous silca's size. Two out of the six tested methods (GEMMA and AF4-ICP-MS) cross validate the MED distributions between each other, providing a true measurement. The measurement accuracy of other four techniques is shown to be compromised either by the high limit of detection and quantification (CLS, NTA, Wet-SEM) or the sample preparation that is biased by increased retention of smaller nanomaterials (SEM). This study thereby presents a successful and conclusive cross-method comparison of size distribution measurements of aggregated nanomaterials. The authors recommend the uniform MED size expression for application in nanomaterial risk assessment studies and clarifications in current regulations and definitions concerning nanomaterials.

Glossary

a	Centrifugal acceleration
AF4-ICP-MS	Assymetric flow field flow fractionation with inductively coupled plasma detection
ANOVA	Analysis of variance
BB8.0	Borate buffer with pH=8.0
C_c	Cunnigham slip correction factor
CLS	Centrifugal liquid sedimentation
D	Diffusion coefficient
D_f	Fractal dimension
d_{pp}	Primary particle diameter
ECD	Equivalent circle diameter
e_e	Elementary charge
EMD	Electrophoretic mobility diameter
ENPs	Engineered nanoparticles
GEMMA	Gas-phase electrophoretic mobility molecular analyzer
HDD	Hydrodynamic diameter
ESD	Equivalent spherical diameter specific to the instrument
k_0	Fractal prefactor of lacunarity
k_B	Boltzmann constant
LOD_s	Limit of detection in relation to particle size
LOQ_s	Limit of quantification in relation to particle size
MALS	Multi angle laser light scattering
MANOVA	Multivariate analysis of variance
MED	Mass equivalent diameter
m	Mass of measured particle or aggregate
N	Number of primary particles within an aggregate
N	Number of electric charges on the particle
NTA	Nanoparticle tracking analysis
p	Statistical significance level (0.05)
PNSD	Particle number size distribution
R_g	Radius of gyration
S	Two dimensional area of particle aggregate projected on microscopy image
SAS	Synthetic amorphous silica
SDD	Sedimentation diameter
SEM	Scanning electron microscopy
T	Temperature
t_r	Retention time in AF4
V_c	Cross-flow volumetric flowrate in AF4
V_{out}	Volumetric outlet flowrate
W	Channel thickness in AF4
Wet-SEM	Liquid scanning electron microscopy
x	Distance from the injection point to the detector in CLS
Z_c	Electric mobility
H	Viscosity of the medium that particle aggregates are suspended in
η_a	Viscosity of air
η_s	Average viscosity of the sucrose gradient in CLS

ρ_f	Average density of the sucrose gradient in CLS
ρ_{pe}	Effective density of particle electric mobility
ρ_{ps}	Effective density of particle sedimentation
ρ_{SiO2}	Density of silica

Introduction

The increasing application of nanotechnology in different industrial sectors, including food and food contact materials, have accelerated the need for the development of reliable techniques for the measurement of submicron sized particles in dispersion [1-4]. Validated analytical methods are not only necessary for quality control and new product development, but also to facilitate risk assessment and risk management under relevant regulations of nanomaterial exposure. One of the pronounced examples for which an accurate measurement of particle size distribution of nanomaterials is necessary is the Food Information Regulation in the European Union which requires labelling of any food products containing nanomaterial additives [5]. This regulation is currently guided by European Commission's recommendation for the definition of a nanomaterial (2011/696/EU). The recommendation defines nanomaterials as materials where "50 % or more of the particles in the number size distribution, one or more external dimensions is in the size range 1 nm-100 nm." [6]. In light of this recommendation some of the existing food additives, especially those produced in sub-micron particle sizes, may be regarded as nanomaterials [7]. A typical example of such material is synthetic amorphous silica (SAS), which is an approved food additive (E551) [8]. The SAS is obtained by burning $SiCl_4$ in a hydrogen/oxygen flame. Single droplets of SiO_2 obtained in the process collide with each other creating stable aggregates [9]. The broad size distribution and complex shape of such aggregated particles poses a particular analytical challenge- ensuring trueness of the obtained measurement [10]. Currently there are no reference materials on the market that would feature aggregated particles. Additionally cross validating measurements of such materials is difficult as use of multiple characterisation techniques

typically yields very different results. There are three main reasons rendering the measurements incomparable in between the analytical methods:

1. The methods for particle size analysis are generally calibrated with or/ and assume in the physical principle ideally spherical particles. However, the physical principles underlying measurements vary in between the methods and shape of SAS aggregates is far from being spherical. Therefore it can be expected that no comparability for size measurements will be achieved for this material, similarly as shown in multiple studies where non-spherical particles were measured by a variety of different analytical methods [11-15].
2. The detection of particles in size distribution generating systems is based on either mass, intensity of scattered/ absorbed light or particle counting. Particle number weighted size distribution (PNSD) can only reflect mass or intensity weighted size distribution if the measured particles are monodispersed spheres. The more the studied material differs from this assumption (in terms of shape or/ and size distribution broadness) the larger the deviations between the size distributions generated by the different detection systems.
3. Generally methods are restricted to the measurement of nano-sized particles down to a certain size. If these sizes are different in between the methods, generated size distributions will be different. Estimation of the minimal detectable particle size for aggregated particles is however not possible if the above first mentioned challenge is not addressed.

In regards to the different particle detection principles, recalculations of mass and intensity based distributions into PNSD are commonly practiced [16-18]. However, the problem of measurement incomparability due to particle non-sphericity seems to be more complex and still presents a challenge.

One way of achieving measurement comparability for non-spherical particles is to transform the results from different analytical methods from that given by the specific instrument equivalent spherical diameter (ESD) into a mass equivalent diameter (MED). The MED is the diameter of a compact sphere having the same mass as the analysed aggregated particle. The dependence of MED on the ESD has previously been described for techniques measuring aerosol particles [19, 20] and might also be applied to engineered nanoparticles (ENPs) in aqueous suspensions. A drawback with adaptation of these previously derived MED relationships [19, 20] is the need for prior knowledge of the dynamic shape factor. Dynamic shape factor is a ratio of drag forces of studied non-spherical particle and theoretical, perfectly spherical particle of the same mass/compact volume as the studied particle [21]. The dynamic shape factor depends on the nature of the flow within the measuring instrument (free molecular, transition or continuum) as well as the specific particle shape. Some values for the dynamic shape factors were derived for differently regularly shaped particles [20], but for the particle aggregates these values were restricted by the arrangement of the particles within the aggregate e.g. chains [19]. Thus, if the arrangement of the particles cannot be described by such simple shapes (as in case of SAS), obtaining a value of dynamic shape factor becomes difficult [22]. Nevertheless, the literature provides some evidence that the ESD can be related to the aggregate fractal structure [23-25] and subsequently to the number of primary particles within such aggregate. Once the number of primary particles within an aggregate is known, the aggregate mass and subsequently MED can be calculated.

The aim of this work was 1) deriving transformations from ESD to MED based PNSDs for 6 methods used frequently for ENP size definition and 2) subsequent application of these transformations for comparison of SAS PNSDs generated by these methods.

Six different techniques were selected to measure SAS. These techniques provided four different types of ESD:

1. Equivalent circle diameter (ECD) – measured by scanning electron microscopy (SEM) and liquid scanning electron microscopy (Wet-SEM);
2. Hydrodynamic diameter (HDD) – measured by nanoparticle tracking analysis (NTA) and asymmetric flow field flow fractionation with inductively coupled plasma detection (AF4-ICP-MS);
3. Sedimentation diameter (SDD) – measured by centrifugal liquid sedimentation (CLS);
4. Electrophoretic mobility diameter (EMD) - measured by gas-phase electrophoretic mobility molecular analyzer (GEMMA).

These 6 methods also covered three different types of particle detection: mass (AF4-ICP-MS), intensity of absorbed light (CLS) and particle counting (SEM, Wet-SEM, NTA, GEMMA). The mass and intensity weighted size distributions were converted into PNSDs to enable comparisons.

The principles of particle measurements for methods applied in this study have previously been described in numerous publications [2, 3, 17, 26- 31]. Thus here only the information helping to understand the derived relationships between ESD's and MED's will be given.

The PNSDs of ENPs except of measurement bias is often affected by the sample preparation [2, 3]. Application of the uniform sample preparation protocol for all analytical methods presented in this study was not possible as these methods operate under very different conditions. Hence, comparison of PNSDs obtained from different methods included also effect of different sample preparations and results where a significant sample preparation effect to PNSD was suspected where accordingly discussed.

This study focused on the measurement of SAS. However, as ENPs tend to lose stability when changes in the suspension state are introduced [32], a separate study was needed to ensure that the measurements on SAS in different instruments were not subject to typical artifacts affecting size distribution, such as aggregation or agglomeration. This study was carried out

using nearly spherical silica ENPs of the same surface chemistry as SAS. Given the shape and narrow size distribution of these ENPs it was possible to directly (without MED transformation) compare the obtained measurements from different instruments and clearly distinguish agglomeration and aggregation. Thanks to this comparison it was also possible to observe the method's constraints for the measurement of spherical silica ENPs under a certain size and assess limits of detection and quantification (LOD_s and LOQ_s). The LOD_s was termed here as smallest detectable particle in the PNSD, and LOQ_s as the size at which the methods registration efficiency started to decrease. This study was carried out in support of the main study presented in the paper and hence was included in Supporting Information, section 1. The results are referred to in the main text where appropriate.

Experimental section

Synthetic amorphous silica

The aqueous dispersion of SAS (AERODISP W 7520 N) was purchased from Evonik (Hanau, Germany). The total silica concentration in the dispersion was at the level of 4%wt and the nominal particle size provided by the manufacturer was 120 nm (static light scattering- Horiba LA 910). The SAS is a fractal aggregate [23], which means that its geometry can be described by the fractal scaling law (Eq. 1) [24].

$$N = k_0 \left(\frac{2R_g}{d_{pp}}\right)^{D_f} \quad \text{Eq. 1}$$

Where:

R_g- radius of gyration

N-number of primary particles within the aggregate

d_{pp}- primary particle diameter

D_f- fractal dimension

k_0- fractal prefactor of lacunarity

The characterisation of the aggregated fractal structure of the SAS is described in Section 2 of the Supporting Information and the experimentally derived parameters are: d_{pp}=9 nm, D_f=2.11 and k_0=1.17.

The SAS dispersion used in this study is not sold for use as a food additive but intended for food applications e.g. clarifying beverages. This SAS was used solely for the analytical method development and this is not an attempt to assess whether the SAS would be regarded a nanomaterial according to EC recommendation [6]. Figure 1 presents an example image of SAS obtained by SEM.

Instruments and measurement conditions

Scanning electron microscopy in high vacuum and liquid setup

SEM and Wet-SEM images were acquired using a FEI Sirion S field emission gun SEM equipped with a through-the-lens detector. The instrument was operated at spot size 3 and voltage of 5kV for high vacuum and at 20 kV for Wet-SEM imaging. Wet-SEM imaging was carried out applying Quantomix™ capsules (QX-102).

The sample preparation and imaging setup for SEM and Wet-SEM was summarised in Supporting Information, section 4. All the analysed images of the same sample in SEM were taken at constant magnification (micrograph size: 3.98 μm^2) where the main particle population was visible. It was noted that for SAS only ENPs up to approximately 300 nm were measured, although a low content of larger particles (up to 1 μm size) was also detected at lower magnification (micrograph size: 29.80 μm^2) in a previous study [33]. The number of these 1 μm particles was so low that the exclusion of this fraction from SAS PNSD could not affect the size values discussed in this study. For Wet-SEM imaging the magnification was limited by the mobility of the particles in the liquid (micrograph size 29.14 μm^2), as we have

found that at increased magnifications, particles would drift away from the membrane within a short time.

All the images for sizing purposes were analysed using an eCognition Architect framework (version 8.7, Trimble Geospatial). A software solution within the eCognition was specifically developed for semi-automated image analysis of aggregated nanoparticles in complex matrices by the Department of GeoInformatics, Paris-Lodron University of Salzburg, Austria as part of the NanoLyse project funded under EU FP7.

Gas electrophoretic mobility molecular analyzer (GEMMA)

A GEMMA (also termed macroIMS (ion mobility spectrometer) or nano-ES (electrospray)-DMA (differential mobility analyser)) system described previously [34] was applied for this study. The stock suspension of SAS was diluted in ratio 1:199 (v/v) with 0.4 M ammonium acetate buffer pH 7.4. Prior to dilution samples were additionally filtered using 0.2 µm Minisart syringe filter (Sartorius, Göttingen, Germany) to avoid clogging the instrument's spray capillary with very large, µm-sized aggregates that by number comprised a negligible fraction of the SAS population [33]. Sample was prepared and analysed in triplicate running seven scans (i.e. resulting in one GEMMA spectrum) per replicate. Median calculation between scans was used for final data presentation. Source flow rates of 0.5 L/min filtered air (table-top compressor, Dürr-Technik, Bietigheim-Bissingen, Germany) and 0.1 L/min CO_2 (99.995%, Air Liquide, Schwechat, Austria) were used for nano-ES and a sheath flow of 3 L/min in the differential mobility separation system. The spray voltage in the nano-ES source was set to 2.5 kV resulting in a current of 500-585 nA. The measurements covered the size range 4.4-163 nm. The PNSD was calculated as described previously [35].

Centrifugal liquid sedimentation

A CPS DC24000 UHR centrifuge (CPS Instruments, Prairieville, LA, USA) operating at a maximum rotational speed of 24,000 rpm was used in this study. The volume of 100 µl of undiluted stock suspension of SAS was analysed in triplicate. Replicates were centrifuged in an 8-24 % sucrose gradient, as specified in the instrument manual [36]. The calibration standard provided by the instrument's manufacturer was used: polyvinyl chloride particles of 476 nm diameter. The density of silica (ρ_{SiO2}) required for the CLS procedure was set at 2.2 g/cm^3 (as recommended by instrument's manufacturer). The effective density of particle sedimentation ρ_{ps}=2.01 g/cm^3 for SAS was provided previously [37].

The run included readings for particle diameter from approximately 700 nm down to the diameter at which negative values for light absorption were obtained. The obtained intensity weighted size distributions were transformed into PNSDs as described previously [17].

Nanoparticle tracking analysis

An NTA instrument LM14 from NanoSight (NanoSight, Amesbury, UK) was used in the study. Samples were diluted with borate buffer at pH 8.0 (BB8.0) of composition: 0.05M H_3BO_3, 0.05M KCl, 0.004M NaOH prior to analysis in a ratio 1:99.999 (v/v) SAS:BB8.0. Samples were prepared in triplicate and 3 recordings per replicate were performed. Recorded videos were 1 min long and were taken at maximal camera shutter and gain settings. Acquired videos were processed with the Nanosight 2.3 software according to the manufacturer's specifications. The raw data output for each single track recorded was used to generate PNSDs presented in the study.

Asymmetric flow field flow fractionation coupled with detection by inductively coupled plasma mass spectrometry

The AF4-ICP-MS system described previously [33] was applied in this study. Size calibration of the AF4 channel was done with NIST traceable latex beads at 50, 100 and 150 nm (Thermo Fisher Scientific, Dreieich, Germany), due to the lack of certified silica reference materials of different sizes. The eluent for size calibration was composed of 0.025% aqueous FL70 (a biodegradable detergent,Fisher Scientific, Waltham, Massachusetts, USA) solution containing 3 mM NaCl (analytical grade, Sigma Aldrich, St. Louis, MO, USA) which was slightly different to one used for separation of SAS (mixture of 0.025% FL70 and 0.25 mM NaCl). This was necessary because the particle behaviour in the channel is strongly related to the surface properties of the particles and so eluent concentration needs to be adjusted to a given material. The elution and analysis conditions were experimentally derived by Stephan Wagner and Samuel Legros from University of Vienna (private communication).

Samples were injected at a concentration of 100 ppm SiO_2 and 50 µl volume in triplicate.

For quality control of AF4 separation, simultaneous measurement of particles eluting from AF4 was performed using multi angle laser light scattering (MALLS). The generated size distributions of SAS were mass-size based and were transformed into PNSD by previously presented calculation [16] assuming spherical particles and ρ_{SiO2}=2.2 g/mL. For MED based distributions this calculation was done following transformation of ESD into MED as described below.

Analysis of synthetic amorphous silica measurements

Comparison of the PNSDs of SAS between the measurement methods was inspired by the methodology used previously [17]. The comparison was achieved using selected percentile size values (5^{th}, 25^{th}, 50^{th}, $75^{th}$and 95^{th}). These were reported together with standard deviations (s.

d.) between replicates. Where raw data (measurements for each single particle) were not available (as in the case of GEMMA, AF4-ICP-MS and CLS) the percentile values were derived from the histograms given by the methods. The data read out from histograms were approximated whilst assuming an even distribution of all the size data points in each bin of the histogram. Given relatively narrow bin width at the values of read percentiles (variable in between the methods and points within the PNSDs from <0.1 to about 2 nm) this approximation had a negligible effect on the result uncertainty. To minimise probability of type I statistical errors, data outputs from all measurement methods were compared for the values of given percentiles using multivariate analysis of variance (MANOVA). If a significant statistical difference was detected ANOVAs followed by relevant post-hoc tests (specified in the result section) were run in order to determine the methods which gave significantly different measurements. All the tests assumed a significance level (p) of 0.05.

Results and discussion

Deriving mass equivalent diameters

The general expression for MED, following the definition given in the introduction of this article represents Eq. 2.

$$MED = \sqrt[3]{\frac{6m}{\pi \rho_{SiO2}}} \qquad \text{Eq. 2}$$

Where:

m- mass of measured particle or aggregate

For ideally spherical particles, MED is equal to particle size measurement directly derived from the instrument. For fractal aggregates, MED calculations were derived using various relationships adapted from the available literature as described below.

Scanning electron microscopy in high vacuum and liquid setup

There is a variety of measurements that can be acquired from analysis of the images, but one of the most common ones is ECD. ECD for a primary or agglomerated particle of area *S* is obtained using Eq. 3

$$S = \pi \left(\frac{ECD}{2}\right)^2 \quad \text{Eq. 3}$$

The relationship between ECD and MED for fractal aggregates was derived using the dependence of the *S* with the number of primary particles within a fractal aggregate (*N*) from EM images [23] (Eq. 4).

$$N = 1.15 \left(\frac{4S}{\pi d_{pp}^2}\right)^{1.09} \quad \text{Eq. 4}$$

Using Eq. 2 and substituting aggregate mass for: $m=N\rho_{SiO2}\frac{\pi d_{pp}^3}{6}$, the relationship of MED with *N* and d_{pp} was obtained (Eq. 5).

$$MED^3 = N\, {d_{pp}}^3 \quad \text{Eq. 5}$$

Substitution of the *N* in Eq. 5 with Eq. 4 and subsequently *S* with Eq. 3 gave the relationship of MED and ECD in Eq. 6.

$$MED = \sqrt[3]{1.15 ECD^{2.18}\, d_{pp}^{0.82}} \quad \text{Eq. 6}$$

Gas-phase electrophoretic mobility molecular analyzer (GEMMA)

The instrument measures electrophoretic mobility of the particles in the gas phase at ambient pressure. Based on this, the spherical equivalent EMD are obtained using Eq. 7 [20].

$$EMD = \frac{n e_e C_c}{3\pi \eta_a Z_c} \quad \text{Eq. 7}$$

Where:

n-number of electric charges on the particle

e_e- elementary charge

C_c- Cunnigham slip correction factor

η_a- viscosity of air

Z_c- electric mobility

The MED of the fractal aggregates can be related to EMD using the general definition for effective density (ρ_{pe}) as in Eq. 8 [20] and calculation of ρ_{pe} related to aggregate's D_f as given in Eq. 9 [25].

$$\rho_{pe}\frac{\pi EMD^3}{6} = \rho_{SiO2}\frac{\pi MED^3}{6} \quad \text{Eq. 8}$$

$$\rho_{pe} = \rho_{SiO2}\left(\frac{EMD}{d_{pp}}\right)^{D_f-3} \quad \text{Eq. 9}$$

Substituting ρ_{pe} in Eq. 8 with Eq. 9, we obtained Eq. 10 describing the relationship of MED and EMD

$$MED = d_{pp}\sqrt[3]{\left(\frac{EMD}{d_{pp}}\right)^{D_f}} \quad \text{Eq. 10}$$

Centrifugal liquid sedimentation

CLS estimates particle SDD based on sedimentation time (t_s) of particles from sample administration to reaching the detector. SDD of the particles is estimated by the instrument's software according to Eq. 11 [36].

$$SDD = \frac{18x\eta_s}{\sqrt[2]{t_s a(\rho_{SiO2} - \rho_f)}} \quad \text{Eq. 11}$$

η_s-average viscosity of sucrose gradient

x- distance from the injection point to the detector

a-centrifugal acceleration

ρ_f- average density of the sucrose gradient

Particle mass concentration is estimated based on light absorption corrected for Mie scattering [38]. The obtained size distribution depends on the particle mass concentration and is then transformed into PNSD by calculation [36]. Any non-spherical shape of the particles slows down their sedimentation velocity when compared to spheres of the same mass. To correct for such velocity change, adjustment of the density value of the particles in Eq. 10 have been suggested [39]. The corrected particle density (ρ_{ps}) can be estimated by means of two CLS measurements in two media of different density. For estimation of ρ_{ps} of the SAS studied here, the so called 'zero velocity approach' was used [37]. This approach is based on Archimedes law. The particle velocity is measured in a medium of lower and higher density than the density of the particle. Then the density of the liquid in which particle would not sediment (have a velocity equal to 0) is calculated. This density is equal to $\rho_{ps.}$ if ρ_{SiO2} in Eq. 11 is substituted with ρ_{ps} then this equation will give the MED value instead of SDD and subsequently Eq. 12 may be derived for relationship of MED and SDD.

$$MED = SSD \sqrt[2]{\frac{\rho_{SiO2} - \rho_f}{\rho_{ps} - \rho_f}} \qquad \text{Eq. 12}$$

It is worth noting that CLS was the only used instrument in this study that was self sufficient in MED determination – as it did not require definition of fractal characteristics of the aggregates from SEM.

Nanoparticle tracking analysis

NTA makes a calculation of the diffusion coefficient (*D*) based on the measurement of an ensemble of absolute mean displacements of individual particles due to the Brownian motion. The *D* is then used to obtain HDD from the Stokes-Einstein dependence (Eq. 13)

$$HDD = \frac{k_B T}{3\pi\eta D} \qquad \text{Eq. 13}$$

Where:

k_B- Boltzmann constant

T- temperature

η- viscosity of suspending medium (here water)

This approach is only suitable for spherical particles (principle of the Stokes-Einstein equation), although there are publications discussing hydrodynamic behavior of fractal aggregates. For example Melas *et al.* (2012) [40] presented relationships between the hydrodynamic radius and R_g of fractal aggregates of specified *N*, D_f and k_0. The provided graphical relationship [40] between R_g and HDD was used to obtain the following relation for the SAS (average N=84±9 and k_0=1.17), Eq. 14

$$HDD = 2.2R_g \qquad \text{Eq. 14}$$

Combining Eq. 1 and Eq. 5 with Eq. 14 a relationship of MED with HDD was obtained (Eq. 15).

$$MED = d_{pp}\sqrt[3]{k_0\left(\frac{HDD}{1.1d_{pp}}\right)^{D_f}} \qquad \text{Eq. 15}$$

Asymmetric flow field flow fractionation with inductively coupled plasma mass spectrometric detection

In AF4, a cross flow drives the particles towards the so-called accumulation wall covered with a membrane. The smaller the particles, the further they diffuse back into the carrier flow channel and form diffusional clouds [41]. The thickness of the clouds depends on the diffusion coefficient D of the particles and the cross flow. A carrier flow along the membrane with a parabolic carrier flow profile makes small particles elute before larger ones. The particle-retention expressed as retention time (t_r) is related to the D of the particles through Eq. 16 [42].

$$t_r = \frac{w^2}{6D} \ln\left(1 + \frac{V_c}{V_{out}}\right) \qquad \text{Eq. 16}$$

Where:

w- channel thickness

V_c- cross-flow volumetric flow rate

V_{out}- volumetric outlet flow rate

Substituting D in Eq. 16 with Eq. 13 the HDD can be calculated according to Eq. 17.

$$HDD = \frac{2t_r k_B T}{\pi \eta w^2 \ln\left(1 + \frac{V_c}{V_{out}}\right)} \qquad \text{Eq. 17}$$

In this study, instead of AF4 theory we applied an independent size measurement by a calibration with particle size standards of known size. This was regarded as a better approach, because the t_r was also shown to be affected by other factors, such as an additional focusing stage after sample injection [31] or particle-membrane interactions, which cannot be avoided

even under close to ideal conditions. Optimization of the AF4 channel for size calibration by standards allows correcting for these additional factors.

Measured by AF4-ICP-MS HDD was transformed into MED according to Eq. 15.

Using MALS coupled to AF4 it was possible to verify the relationship between HDD and R_g. Ratios between HDD/R_g ranged from 2.0 to 2.34 through the entire PNSD of SAS. This proved that the 2.2 value adapted from the reference [40] in Eq. 14 was a very good approximation.

Application of mass equivalent diameter for comparison of particle number-size distributions of SAS as characterised by different analytical techniques

Measurement comparability between techniques after data transformation into mass equivalent diameter

As expected, PNSDs of SAS obtained directly from measurements or after calculations reported as ESD (Figure 2A, Figure 3A, Table 1) differed widely depending on the analytical technique. The broadest and the narrowest ESD weighted PNSD were obtained by NTA and CLS, respectively with differences between the 95th and 5th percentile of 182 nm for NTA and 53 nm for CLS. SAS median sizes were in the range of 40 nm for SEM to 115 nm for NTA. Shapes of the curves were also found to vary widely with NTA and Wet-SEM displaying an approximately normal PNSDs and CLS, GEMMA and AF4-ICP-MS showing positively skewed PNSDs. The variation in PNSDs shape may suggest variable efficiency of the methods for detecting small nanomaterials, but also may be a result of different measurement expression.

Table 1. Mode, percentile diameter and respective standard deviations (in brackets) in PNSD of SAS given as ESD in nm

Method	5%	25%	Mode	50%	75%	95%
SEM (ECD)	10 (0)^{A}	22 (2)^{A}	14 (3)	40 (3)^{A}	68 (3)^{A}	124 (6)^{A}
GEMMA (EMD)	16 (1)^{A}	44 (2)^{B}	72 (3)	66 (1)^{B}	91 (1)^{B}	131 (1)^{AB}
CLS (SDD)	30 (1)^{B}	38 (1)^{C}	42 (3)	47 (1)^{AC}	59 (1)^{A}	83 (1)^{A}
AF4-ICP-MS (HDD)	16 (3)^{A}	40 (0)^{BC}	45 (7)	56 (1)^{BC}	79 (0)^{AB}	123 (1)^{A}
NTA (HDD)	43 (3)^{C}	82 (4)^{D}	157 (37)	115 (5)^{D}	153 (6)^{C}	226 (8)^{C}
Wet-SEM (ECD)	62 (4)^{D}	85 (2)^{D}	95 (3)	104 (8)^{E}	127 (14)^{D}	182 (58)^{BC}

$^{A-F}$Same letter in column with percentile size value in Table 1 and 2 means that no significant difference between measurement results was detected (Tukey's test, p>0.05).

Transformation of the ESD into MED (Figure 2B, Figure 3B, Table 2) resulted in narrowing PNSD for all the methods with exception of CLS (difference between 95th and 5th percentile for ESD 53 nm, for MED 57 nm). The difference between 95th and 5th percentile in MED distributions was ranging from 43 to 59 nm among the measurement methods and was smallest for AF4-ICP-MS and largest for NTA.

Table 2. Mode, percentile diameter and respective standard deviations (in brackets) in PNSD of SAS given as MED in nm

Method	5%	25%	Mode	50%	75%	95%
SEM	11 (0)^{A}	18 (1)^{A}	13 (2)	28 (1)^{A}	41 (1)^{A}	64 (2)^{A}
GEMMA	13 (1)^{A}	28 (1)^{B}	39 (0)	37 (0)^{B}	46 (0)^{AB}	59 (0)^{A}
CLS	32 (1)^{B}	41 (1)^{C}	44 (1)	51 (1)^{C}	63 (1)^{C}	90 (1)^{B}
AF4-ICP-MS	21 (0)^{C}	30 (0)^{B}	33 (1)	38 (0)^{B}	47 (0)^{B}	64 (0)^{A}
NTA	27 (1)^{D}	42 (1)^{C}	66 (11)	54 (2)^{CD}	65 (2)^{C}	86 (2)^{B}
Wet-SEM	39 (2)^{E}	48 (1)^{D}	52 (1)	56 (3)^{D}	64 (5)^{C}	84 (19)^{B}

$^{A-F}$As in Table 1

Best correspondence of MED transformed PNSDs was achieved for GEMMA and AF4-ICP-MS (Table2; Figure 2B, Figure 3 B). The PNSDs of SAS from these two methods were in a good agreement already for ESD measurements (Figure 2A, Figure 3A and Table 1), however the transformation improved the comparability of these results especially in the central part of the curve (Figure 2 and 3). This can be noticed looking also at the difference of median diameter between GEMMA and AF4-ICP-MS measurements in Tables 1 and 2,

which decreased after MED transformation from 14 to 3% (relative to the GEMMA given median).

After MED transformation, the Wet-SEM, NTA and CLS generated PNSDs were shifted toward larger MED values in comparison to AF4-ICP-MS and GEMMA ones (Figure 2B). These three methods measured median MED of SAS similarly (56; 53 and 51 nm respectively) (although Tukey's test, $p<0.05$ for CLS and Wet-SEM, indicating statistically significant difference). Only the SAS median MED generated by SEM was not comparable to that given by any other measurement technique, showing MED significantly smaller (Tukey's test, $p<0.05$).

There are several reasons for not achieving complete comparability between PNSDs generated by different analytical methods after MED transformation and these are discussed below.

Limits of detection and quantification and procedural artefact affecting PNSD of SAS in different measurement instruments

All the methods were limited in detection of SAS ENPs down to a certain size. In GEMMA and AF4-ICP-MS measurement of SAS ENPs was restricted to particle sizes >13-18 nm MED. In AF4-ICP-MS measurement of particles with a smaller size became inaccurate under the applied analytical conditions due to the background noise. In GEMMA interferences from e.g. residual dissolved non-volatile substances posed restrictive factor. These effects were also observed during analysis of spherical silica ENPs (Supporting Information, section 1) but in a smaller size region (AF4-ICP-MS measured small spherical silica ENPs down to 7 nm and GEMMA to 8 nm without interference). SEM and Wet-SEM were limited to measurement of SAS particles larger than 8 nm and 32 nm respectively due to the chosen size cut-off point. CLS detected SAS ENPs only down to 27 nm and NTA down to 8 nm. These results are in disagreement with what we have observed for spherical silica ENPs (Supporting

Information, section 1). Spherical silica ENPs could be detected down to 23 nm by NTA and 9 nm in CLS, although in case of CLS the result was not reproducible. These discrepancies could be a result of differences in light scattering by non-spherical SAS when compared to spherical ENPs in NTA and lower mass concentration of analysed SAS to spherical ENPs in CLS. The result emphasizes the difficulties in unambiguous determination of the LOD_s that could be generalized for silica ENPs.

The three methods which measured median SAS MED above 50 nm - CLS, Wet-SEM and NTA displayed a gradual loss of particle detection efficiency prior to reaching respective LOD_s. This effect was also clearly observed while measuring spherical silica ENPs with bimodal size distribution (see Supporting Information, section 1). All 3 methods discriminated number of spherical silica ENPs in smaller size population (18-62 nm) on account of larger size population (63-106 nm) in comparison to chosen reference method for accurate particle count- GEMMA. The LOQ_s can be determined from the modal SAS MED value of the PNSDs of the respective measurement techniques (see Table 2). Values of LOQ_s for CLS, NTA and Wet-SEM were 44 nm, 66 nm, and 52 nm respectively. Determined LOQ_s for NTA in SAS MED measurement was characterised by a large standard deviation and thus value was in agreement to LOQ_s determined for small spherical silica (see Supporting Information, section 1). For the other two techniques we did not obtain such comparability, thus it can be concluded that the estimation of size LOQ_s generally for silica ENPs might be as challenging as in case of LOD_s.

The reason for appearing of LOQ_s in SAS PNSDs generated by NTA, CLS and Wet-SEM is not fully understood. It could be expected that if the method measures only the tail of the true PNSD the modal size value will equal to the smallest detected particle size, as shown e.g. for ENPs measured with single particle ICP-MS [43]. Some authors suggested that methods can only measure particles accurately down to a certain size point [44]. Nevertheless by analysing

the bimodal PNSD of spherical silica (Supporting Information, Section 1) we have shown that at least in the case of CLS the problem lays in a reduced detection efficiency towards diminishing particle size rather than inacurate measurement of small particles.

The particle detection in CLS and NTA relies on light scattering and absorption respectively. It is a common knowledge that silica scatters and absorbs light poorly hence being difficult in detection for such methods [36, 44].

The justification for detection of LOQ_s in the Wet-SEM generated PNSD of SAS still requires further experimental examination. Based on the results presented here and observations during data acquisition (summarised in Supporting Information, section 4) the aggregates smaller than LOQ_s SAS could have been more prone to drift away from the imaging membrane. For Wet-SEM images (see Supporting Information, section 4) the unavoidable image blur could contribute to decreased detection efficiency of particles smaller than 52 nm.

The instrument in which characterisation of PNSD seemed to be affected by sample preparation (see Supporting Information, section 1 for discussion) was SEM. We showed in Supporting Information section 1, that SEM was able to measure spherical silica ENPs characterised by a narrow PNSDs comparably to GEMMA. But when measuring a sample of spherical silica ENPs featuring broad, bimodal PNSD the SEM overestimated counts of small particles. This artefact was attributed to sample preparation and was suspected by different authors earlier [45-47]. The sample preparation required for electron microscopy most often also causes particle agglomeration [2]. Agglomeration artefact disables measurement of the particle aggregates. The sample preparation method chosen here, as mentioned in Supplementary Information, section 4, was evaluated among others and was most effective in minimizing agglomeration of silica ENPs, but as shown here at a cost of another artefact- erroneous increase of particle abundance with decrease of size:

Trueness of median measurements of SAS

The question that remains to be answered is which of the methods most accurately characterised the PNSD of SAS. Despite contamination interferences in the small size region, GEMMA and AF4-ICP-MS data outputs cross validated each other. Furthermore GEMMA is known for an accurate particle count [48] and we confirmed that it measured the size of spherical silica ENPs accurately (Supporting Information, section 1). These findings indicate that AF4-ICP-MS and GEMMA characterised PNSD of SAS most accurately among compared methods. Such good correspondence of the PNSDs measurements for aggregated ENPs between two methods underlying different measurement principles to our knowledge has not been previously reported. In fact, validation of PNSDs of ENPs by use of independent measurement methods so far has been perceived as not possible [49]. Contrary to this perception, achieved here preliminary (as not yet fully validated) success of the approach for calculation of the uniform measurement expression allows to think that the trueness assessment can be obtained.

Remaining analytical methods were deviating from true median SAS MED given by GEMMA (37 nm) and AF4-ICP-MS (38 nm) in a following order: SEM<CLS<NTA<Wet-SEM. Calculated trueness values for median SAS measurements for these four methods were very poor (ranging 24-51%- given as a absolute difference between reference (37 nm) and investigated median MED, relatively to the reference median MED). Due to this large trueness error we cannot currently recommend these methods for SAS measurement. Further research into improvements of detection systems and sample preparation could change this recommendation.

Conclusions

There is a number of available sizing techniques for ENPs in suspension. However, direct comparison of the measurements between methods that provided different size parameters for irregularly shaped, aggregated ENPs was so far not possible. Therefore, here a set of relationships allowing conversion of the different size parameters into a uniform expression-MED was developed. The MED expressed PNSDs of SAS for six analytical methods were compared and we found that:

1. GEMMA and AF4-ICP-MS cross validated PNSD of SAS given as MED between each other
2. CLS, Wet-SEM and NTA suffered from lowered particle counting/ detecting efficiency after achieving MED of 44-66 nm
3. Sample preparation for SEM caused the method to overestimate small particle counts, resulting in a reduction of SAS median MED
4. LOD_s and LOQ_s for size of SAS did not generally match with spherical silica ENPs characterised in the Supplementary Information, section 1. These effects were attributed not only to particle shape, but also the presence of residual substances in the samples and mass concentrations of the ENPs. Thus in the worst case scenario LOD_s and LOQ_s might be sample specific.
5. High trueness error of SAS median MED measurement associated with four of the tested methods: SEM, CLS, NTA and Wet-SEM indicated that further optimization of these methods for SAS measurement is required

The MED is one of the possible ways of interpreting the data outputs from different measurement techniques.

It is worth emphasising that out of six tested here methods CLS can be used to obtain MED expressed size distribution without the necessity of knowing the particle fractal structure. Another method that could be recommended for the measurement of MED is single particle-ICP-MS. This method allows to measure MED directly, but has not been used in this study due to high expected LOD_s making measurement of silica ENPs not possible [50]. Both CLS and single particle ICP-MS in current state of the art could be recommended for further validation of aggregated ENPs' MED. That is as long as the size and chemical composition of particular aggregated ENPs do not hamper the full characterisation of PNSD.As presented in this study, MED enables comparison and validation of the measurement results for aggregated ENPs featuring broad PNSD. It should be noted that this paper documents only a preliminary success of MED calculation approach applied for method validation purposes and sets a new standard, yet to be more rigorously tested.

Use of MED could aid development of reference materials featuring aggregated ENPs. Such reference materials are needed for the validation of analytical methods measuring aggregated ENPs in environmental matrices and industrial products.

In summary we would recommend MED for use as a uniform expression of particle size measurements in support of future research and regulations on nano-sized or nano-structured materials in dispersion.

Acknowledgements

The authors would like to acknowledge Dr Samuel Legros from the University of Vienna for his work on development AF4-ICP-MS for analysis of silica ENPs. We are also grateful to Dr Thomas Linsinger from Joint Research Centre, Institute for Reference Materials and Measurements (Geel, Belgium) for providing SAS study material. We would like to also acknowledge directors and staff of The University of York's JEOL Nanocentre for technical

help and facilitated access to the electron microscopes. This work received financial support from EU Seventh Framework Programme NanoLyse (FP7/2007-2013) under grant agreement n° 245162.

Supporting Information Available: This material is available free of charge via the Internet at http://pubs.acs.org.

References

1 D. M. A. M. Luykx, R. J. B. Peters, S. M. van Ruth and H. Bouwmeester, *J. Agric. Food Chem.,* 2008, **56**, 8231–8247.

2 K. Tiede, A. Boxall, S. Tear, J. Lewis, H. David and M. Hassellov, *Food Addit. Contam. Part A*, 2008, **25**, 795–821.

3 A. Dudkiewicz, P. Luo, K. Tiede and A. B. A. Boxall, in *Nanotechnology in the food, beverage and nutraceutical industries*, ed. Q. Huang, Woodhead Publishing, Cambridge, 2012, ch. 3, pp. 53–80.

4 S. Bandyopadhyay, J. R. Peralta-Videa and J. L. Gardea-Torresdey, *Environ. Eng. Sci.*, 2013, **30**, 118–125.

5 European Commission, Communication from the Commission to the European Parliament, the Council and the European Economic and Social Commitee, 2012, **COM (2012) 572**, http://ec.europa.eu/research/industrial_technologies/pdf/policy/communication-from-the-commission-second-regulatory-review-on-nanomaterials_en.pdf, (accessed July 2014).

6 The European Commission, *Official Journal of the European Union*, 2011, **275**, 38–40.

7 Q. Chaudhry and K. Groves, in *Nanotechnologies in Food*, ed. Q. Chaudhry, L. Castle and R. Watkins, RSC Publishing, London, 2010, ch. 5, pp. 69–84.

8 S. Dekkers, P. Krystek, R. J. B. Peters, D. P. Lankveld, B. G. Bokkers, P. H. van Hoeven-Arentzen, H. Bouwmeester and A. G. Oomen, *Nanotoxicology*, 2010, **5**, 393–405.

9 H. Barthel, M. Heinemann, M. Stintz and B. Wessely, *Part. Part. Syst. Charact.*, 1999, **16**, 169–176.

10 A. Dudkiewicz, A. B. A. Boxall, Q. Chaudhry, K. Mølhave, K. Tiede, P. Hofmann and T. P. J. Linsinger, *Food Chem.*, 2015, **176**, 472–479.

11 P. Bowen, *J. Dispersion Sci. Technol.*, 2002, **23**, 631–662.

12 R. F. Domingos, M. A. Baalousha, Y. Ju-Nam, M. M. Reid, N. Tufenkji, J. R. Lead, G. G. Leppard and K. J. Wilkinson, *Environ. Sci. Technol.*, 2009, **43**, 7277–7284.

13 M. Staiger, P. Bowen, J. Ketterer and J. Bohonek, *J. Dispersion Sci. Technol.*, 2002, **23**, 619-630.

14 A. Aimable and P. Bowen, *Process. Appl. Ceram.*, 2010, **4**, 157-166.

15 P. Bowen, J. Sheng and N. Jongen, *Powder Technol.*, 2002, **128**, 256-261.

16 R. J. B. Peters, G. van Bemmel, Z. Herrera-Rivera, H. P. F. G. Helsper, H. J. P. Marvin, S. Weigel, P. C. Tromp, A. G. Oomen, A. G. Rietveld and H. Bouwmeester, *J. Agric. Food Chem.*, 2014, **62**, 6285–6293.

17 W. Anderson, D. Kozak, V. A. Coleman, Å. K. Jämting and M. Trau, *J. Colloid Interface Sci.*, 2013, **405**, 322–330.

18 H. Hinterwirth, S. K. Wiedmer, M. Moilanen, A. Lehner, G. Allmaier, T. Waitz, W. Lindner and M. Lämmerhofer, *J. Sep. Sci.*, 2013, **36**, 2952–2961.

19 G. Kasper, *Aerosol Sci. Technol.*, 1982, **1**, 187–199.

20 P. F. DeCarlo, J. G. Slowik, D. R. Worsnop, P. Davidovits and J. L. Jimenez, *Aerosol Sci. Technol.*, 2004, **38**, 1185–1205.

21 Y. S. Cheng, H. C. Yeh and M. D. Allen, *Aerosol Sci. Technol.*, 1988, **8**, 109–123.

22 A. Zelenyuk, Y. Cai and D. Imre, *Aerosol Sci. Technol.*, 2006, **40**, 197–217.

23 D. Boldridge, *Aerosol Sci. Technol.*, 2010, **44**, 182–186.

24 L. Gmachowski, *Colloids Surf., A*, 2000, **170**, 209–216.

25 M. M. Maricq and N. Xu, *J. Aerosol Sci.*, 2004, **35**, 1251–1274.

26 G. Bacher, W. W. Szymanski, S. L. Kaufman, P. Zollner, D. Blaas and G. Allmaier, *J. Mass Spectrom.*, 2001, **36**, 1038–1052.

27 K. Tiede, S. P. Tear, H. David and A. B. A. Boxall, *Water Res.*, 2009, **43**, 3335–3343.

28 A. Braun, O. Couteau, K. Franks, V. Kestens, G. Roebben, A. Lamberty and T. P. J. Linsinger, *Adv. Powder Technol.*, 2011, **22**, 766–770.

29 T. P. J. Linsinger, G. Roebben, D. Gilliland, L. Calzolai, F. Rossi, N. Gibson and C. Klein, 2012, http://publications.jrc.ec.europa.eu/repository/bitstream/111111111/26399/2/irmm_nanomaterials%20%28online%29.pdf, (accessed June 2014).

30 B. Carr and A. Malloy, http://www.me.umn.edu/centers/cdr/reports/NanoSightPaper.pdf, (accessed June 2014).

31 K. Loeschner, J. Navratilova, S. Legros, S. Wagner, R. Grombe, J. Snell, F. von der Kammer and E. H. Larsen, *J Chromatogr A*, 2013, **1272**, 116–125.

32 S. Park, J. Woodhall, G. Ma, J. G. Veinot, M. S. Cresser and A. B. Boxall, *Nanotoxicology*, 2013, 1–10.

33 R. Grombe, J. Charoud-Got, H. Emteborg, T. P. J. Linsinger, J. Seghers, S. Wagner, F. von der Kammer, T. Hofmann, A. Dudkiewicz, M. Llinas, C. Solans, A. Lehner and G. Allmaier, *Anal. Bioanal. Chem.*, 2014, **406**, 3895–3907.

34 V. U. Weiss, X. Subirats, A. Pickl-Herk, G. Bilek, W. Winkler, M. Kumar, G. Allmaier, D. Blaas and E. Kenndler, *Electrophoresis*, 2012, **33**, 1833–1841.

35 A. G. Hallar, G. Chirokova, I. McCubbin, T. H. Painter, C. Wiedinmyer and C. Dodson, *Geophys. Res. Lett.*, 2011, **38**, L17801.

36 CPS Instruments, Inc., 2005, http://www.cpsinstruments.eu/pdf/Manual.pdf, (accessed June 2014).

637 37 H. Woehlecke, D. Lerche, T. Detloff, K. Franks, V. Kestens and G. Roebben, *International Congress on Particle Technology (PARTEC) Abstracts and Proceedings*, 2013, Abstract No. 488.

640 38 T. Wriedt, in *The Mie theory basics and application.*, ed. W. Hergert and T. Wriedt , Springer, Georgia, 2012, ch. 2, pp. 53–71.

642 39 M. Kamiti, D. Boldridge, L. M. Ndoping and E. E. Remsen, *Anal. Chem.*, 2012, **84**, 10526–10530.

644 40 A. D. Melas, A. G. Konstandopoulos, L. Isella and Y. Drossinos, *Excerpt from the Proceedings of the 2012 COMSOL Conference in Milan*, 2012, http://www.comsol.com/offers/conference2012papers/papers/file/id/13411/file/14627_melas_paper.pdf, (accessed June 2014).

648 41 F. A. Messaud, R. D. Sanderson, J. R. Runyon, T. Otte, H. Pasch and S. K. R. Williams, *Prog. Polym. Sci.*, 2009, **34**, 351–368.

650 42 K. G. Wahlund and J. C. Giddings, *Anal. Chem.*, 1987, **59**, 1332–1339.

651 43 F. Laborda, J. Jiménez-Lamana, E. Bolea and J. R. Castillo, *J. Anal. At. Spectrom.*, 2013, **28**, 1220-1232.

653 44 J. Tuoriniemi, A. C. J. H. Johnsson, J. P. Holmberg, S. Gustafsson, J. A. Gallego-Urrea, E. Olsson, J. B. C. Pattersson and M. Hassellöv, *Sci. Technol. Adv. Mater.*, 2014, **15**, 035009.

655 45 M. Baalousha and J. R. Lead, *Environ. Sci. Technol.*, 2012, **46**, 6134-6142.

656 46 E. Balnois and K. J. Wilkinson, *Colloids and Surf., A*, 2002, **207**, 229–242.

657 47 P. Luo, I. Morrison, A. Dudkiewicz, K. Tiede, E. Boyes, P. O'Toole, S. Park and A. B. Boxall, *J. Microsc.*, 2013, **250**, 32–41.

659 48 J. Kesten, A. Reineking and J. Porstendörfer, *Aerosol Sci. Technol.*, 1991, **15**, 107–111.

49 T. P. J. Linsinger, Q. Chaudhry, V. Dehalu, P. Delahaut, A. Dudkiewicz, R. Grombe, F. von der Kammer, E. H. Larsen, S. Legros, K. Loeschner, R. Peters, R. Ramsch, G. Roebben, K. Tiede and S. Weigel, *Food Chem.*, 2013, **138**, 1959–1966.

50 S. Lee, X. Bi, R. B. Reed, J. F. Ranville, P. Herckes and P. Westerhoff, *Environ. Sci. Technol.*, 2014, **48**, 10291–10300.

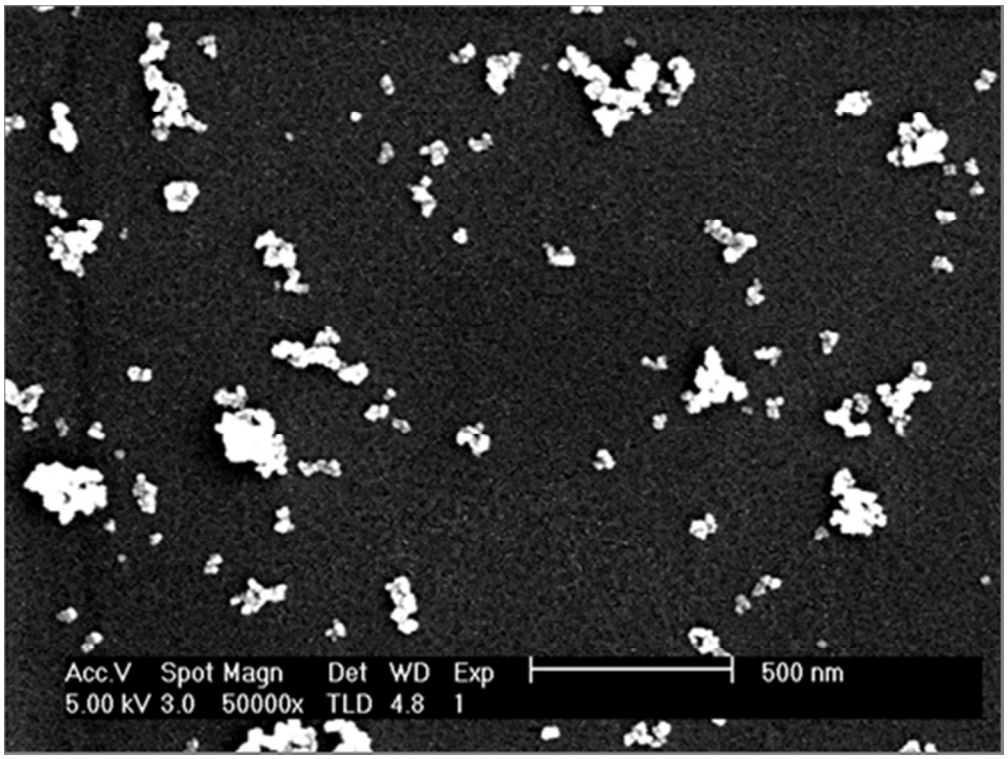

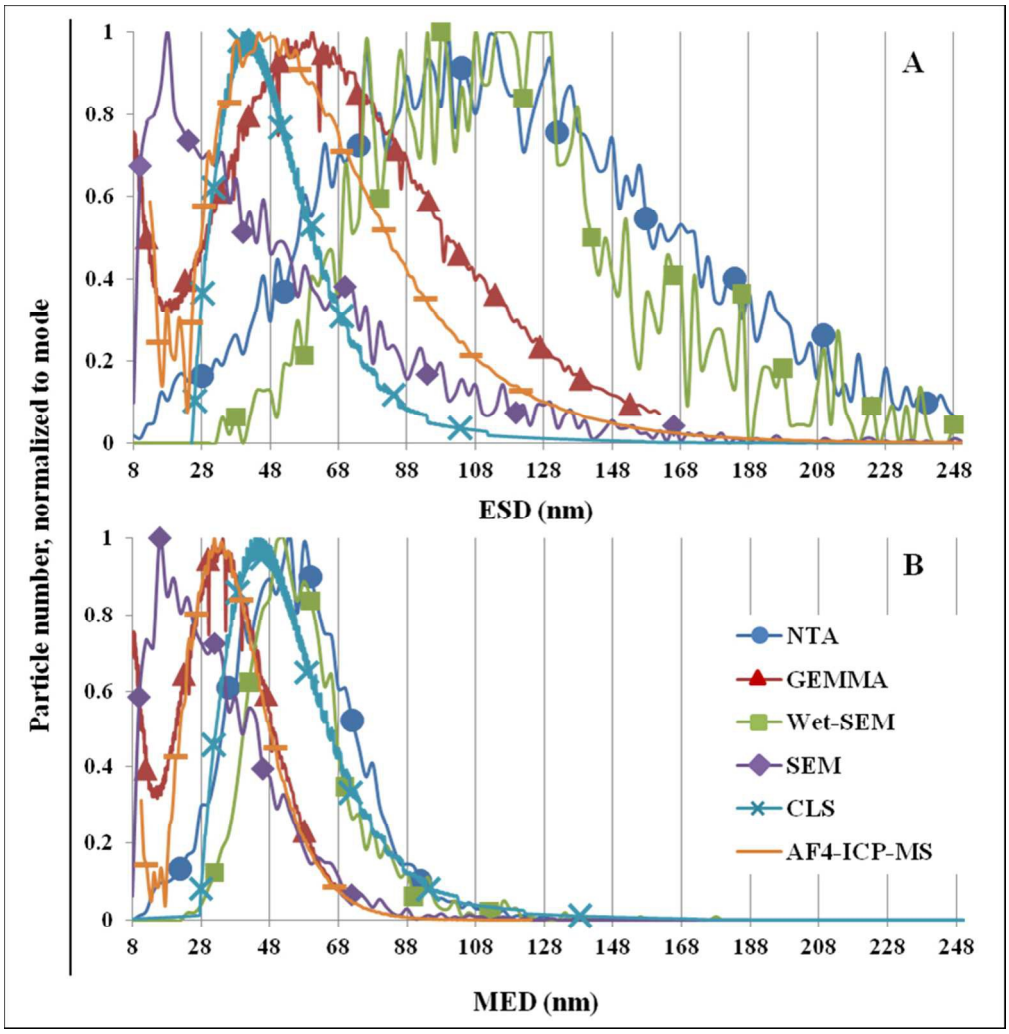

154x158mm (150 x 150 DPI)

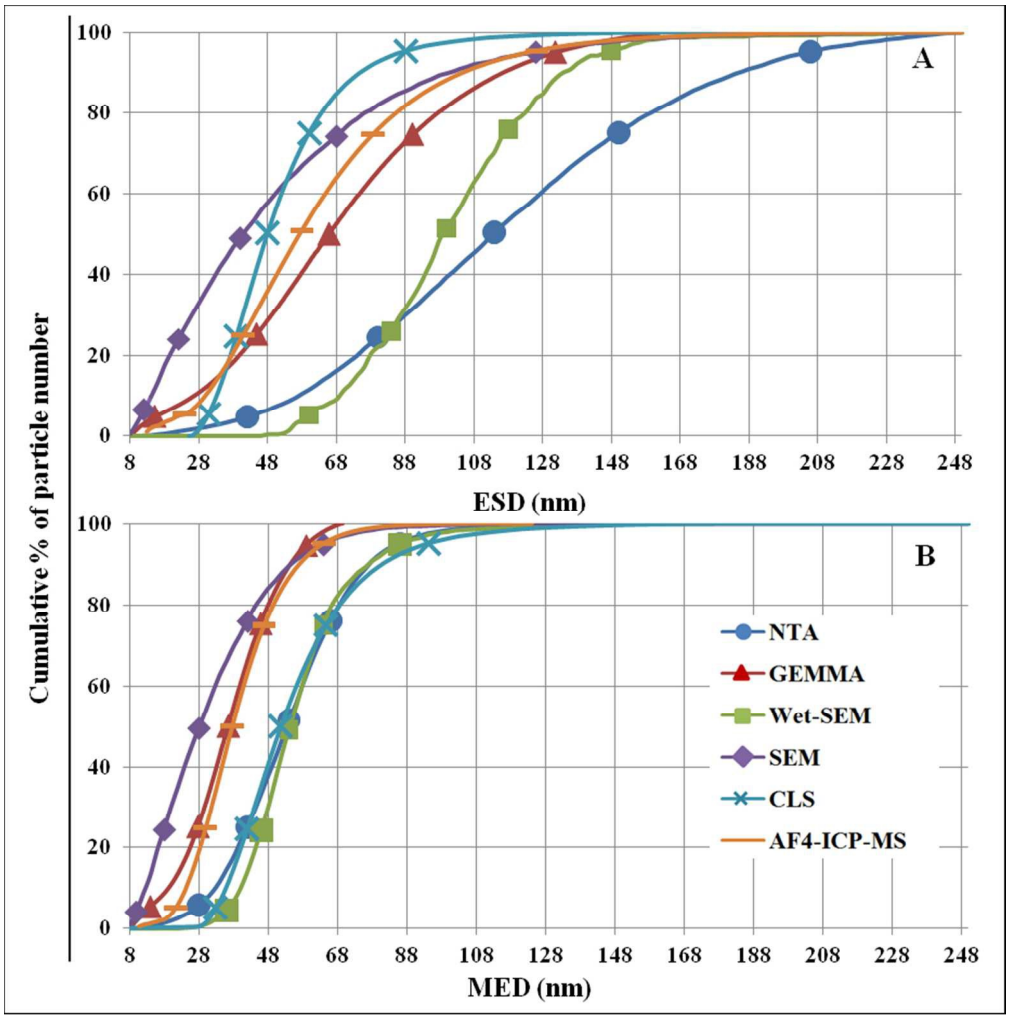

156x157mm (150 x 150 DPI)

Figure 1. SEM image of SAS, scale bar is 500 nm

Figure 2. PNSD of SAS (A) expressed as ESD, (B) expressed as MED

Figure 3. Cumulative percentage distribution of particle size in PNSD (A) expressed as ESD , (B) expressed as MED